Theor Chim Acta (1992) 82: 357–382

Theoretica Chimica Acta

Role of monomer structure and compressibility on the properties of multicomponent polymer blends and solutions

IV. High molecular weights, temperature dependences, and phase diagrams of binary polymer blends

Karl F. Freed and Jacek Dudowicz

The James Franck Institute and the Department of Chemistry, University of Chicago, Chicago Il 60637, USA

Received March 6, 1991/Accepted June 10, 1991

Summary. The lattice cluster theory of corrections to Flory–Huggins theory is applied to binary compressible blends (at a pressure of one atmosphere) that are formed by polymers having structured monomers. Calculations are performed in the high molecular weight limit for the dependence of the small angle neutron scattering effective interaction parameter χ_{eff} on composition Φ_1, monomer structure, microscopic interaction energies, and temperature. The limiting high molecular weight $\chi_{eff}(\Phi_1)$ curves have an overall general parabolic behavior with center, curvature, and magnitude that vary significantly with monomer structures and with interaction energies. The latter variation is stronger and occurs even at constant Flory–Huggins interaction parameter χ_{12}^{FH} where incompressible blend models cannot describe the strong dependence on the self-polymer-polymer-interactions obtained here. A quasi-athermal limit, in which $\chi_{eff}(\Phi_1)$ is nearly temperature independent, appears for high molecular weights only when χ_{12}^{FH} is vanishingly small. Phase diagrams are studied by evaluating the cloud points for coherent scattering from binary blends. Blends with negative χ_{12}^{FH} have only a LCST, but ones with positive χ_{12}^{FH} may have closed loop phase diagram or both LCST and UCST. However, one of the latter two critical points may be unobservable due to an intervening glass transition or because of thermal degradation.

Key words: Polymer blends – Monomer structure – Compressibility – Lattice theory – Phase diagrams

1. Introduction

Polymers are essential components in all biological systems and in a wide variety of advanced materials. Polymers may be found in solutions, as liquids, glasses, crystalline materials, micelles, liquid crystals, and gels. They may be studied in static or flowing systems and under equilibrium or highly nonequilibrium conditions. The rich variety of phenomena associated with polymers is now accepted to be a direct consequence of the extended nature and internal flexibility of polymer chains.

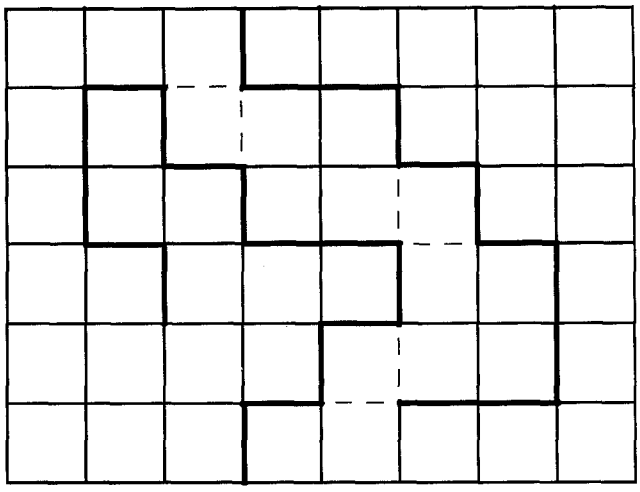

Fig. 1. Examples of two short linear polymer chains of species 1 and 2, with $N_1 = 12$ and $N_2 = 16$ monomers, respectively, on a square lattice ($z = 4$). Nearest neighbor monomers interact with attractive van der Waals energy ε_{ij} $(i, j = 1, 2)$. Dashed lines represent the interactions between monomers of different polymer species

Early theoretical studies of polymers [1] centered on the description of their properties in dilute solutions [2], on the one hand, and in concentrated solutions or the liquid state (called the melt) on the other hand. Meyer [3] first suggested that the entropy of mixing for long-chain polymers with small solvent molecules could be calculated by using a lattice model in which the monomers of the polymer chain occupy the same kind of sites as solvent molecules. This model is depicted in Fig. 1 with two polymer chains of different polymer species on a square lattice. The polymers of a given species are represented in Fig. 1 by sequentially bonded sets of monomer units such that no two monomers occupy the same lattice site. All sites not occupied by polymers are taken by solvent molecules for concentrated polymer solutions, or they remain empty and thus model excess free volume in treatments of compressible polymer systems. Figure 1 presents the polymer chains as being completely flexible. This model therefore represents the polymers as self and mutually avoiding random walks on a lattice. Computation of the systems' (athermal limit) packing entropy proceeds according to the usual statistical mechanical definition relating the entropy to the total number of configurations available to the system.

The lattice model also includes attractive van der Waals interaction energies between nonbonded nearest neighbors. Those involving monomers of different polymer species are depicted by dashed lines in Fig. 1. A binary polymer blend has the three attractive interaction energies ε_{11}, ε_{22}, and ε_{12} between the respective nearest neighbors lattice pairs. The introduction of these interaction energies enables computations of all thermodynamic properties for polymeric systems.

The counting problem posed by the enumeration of all configurations available to self and mutually avoiding polymers on a lattice has been formidable [1, 4–6]. The mean-field treatments of Flory [1, 7–9] and Huggins [10] for long, linear, flexible polymers represented a major breakthrough in providing what has become probably the most widely used theory for the thermodynamic properties of polymer systems. These lattice models have played an important role in developing statistical mechanical theories of, for example, polymer solutions [1], gels [11], the polymer glass transition [12], liquid crystals [13–17], rubber elasticity [18, 19], and the segregation of two or more polymer species [20, 21].

Standard Flory–Huggins mean-field approximations replace the strict constraint of single occupancy at each lattice site by probabilistic arguments for the site occupancy [1]. As an illustration, the Helmholtz free energy of mixing ΔF^{mix} for two kinds of polymers in the incompressible liquid phase (called a blend) emerges in the well-known form involving a combinatorial entropy and an energy of mixing [1]:

$$\frac{\Delta F^{mix}}{N_l k_B T} = \frac{\phi_1}{M_1} \ln \phi_1 + \frac{\phi_2}{M_2} \ln \phi_2 + \chi_{12}^{FH} \phi_1 \phi_2, \tag{1.1}$$

where N_l is the total number of lattice sites, ϕ_i is the fraction of sites occupied by species i (usually called the segment fraction), and M_i is the number of lattice sites occupied by a single chain of type i. The Flory–Huggins theory interaction parameter χ_{12}^{FH} is obtained from the nearest neighbor attractive neighbor van der Waals energies ε_{ij} as:

$$\chi_{12}^{FH} = z(\varepsilon_{11} + \varepsilon_{22} - 2\varepsilon_{12})/(2k_B T), \tag{1.2}$$

where z is the number of nearest neighbors to a given lattice site (called the lattice coordination number). In practice, χ_{12}^{FH} in Eq. (1.1) is treated as a phenomenological parameter, and the free energy of mixing then becomes independent of any lattice model parameters. Flory obtained Eq. (1.1) by sequentially placing uncorrelated, but connected, monomers on the lattice, whereas Huggins used a more sophisticated counting scheme which begins to account for the short-range correlations associated with individual bonds [22]. The Huggins approach differs from Flory's by a small additional contribution to the entropy of mixing that depends explicitly on the lattice coordination number z. Lack of knowledge of the appropriate value of the z for realistic polymer systems and the greater simplicity of the Flory one-parameter theory led to the widespread use of the Flory form [Eq. (1.1)], which has been termed Flory–Huggins theory to respect the independent contributions of Huggins.

The mean-field expression of Eq. (1.1) displays a blend as having a very small entropy of mixing because of the high polymer molecular weights, i.e., the large number of segments M_i on a single polymer. In addition, estimates of the interaction energies ε_{ij} from molecular polarizabilities lead to the expectation that χ_{12}^{FH} in Eq. (1.2) is generally positive, giving an unfavorable heat of mixing. Consequently, the Flory–Huggins prediction of Eq. (1.1) implies that long-chain, flexible polymers would not tend to mix in the liquid state, and this is generally observed. However, blends are useful as precursors to a variety of composite materials, so considerable effort has been devoted to find polymers that mix (blend) in the liquid state and to find some principles guiding polymer mixing. Unfortunately, standard Flory–Huggins theory of Eqs. (1.1) and (1.2) and its straightforward generalizations offer no such guidance.

The Flory formulation in Eq. (1.2) displays the interaction parameter χ as independent of composition and molecular weights, proportional to T^{-1}, and energetic in origin. However, when χ is treated as a phenomenological parameter, comparisons with experiment show χ to depend on polymer concentration and molecular weights and to contain both energetic and entropic contributions [1, 22–26]. Often the entropic contribution to χ greatly exceeds the enthalpic one. These empirical observations strongly conflict with the predictions derived from the original model and leading to Eqs. (1.1) and (1.2). Therefore, there must be errors in either the lattice model, the mean-field approximation of Flory, or both. The improved counting scheme of Huggins provides an entropic

contribution to χ that is too small in magnitude to explain the experimental results. Koningsveld and Kleitjens [27] and Kurata et al. [28] have applied Guggenheim [29]–Huggins-type counting arguments to the energetic term χ in Eq. (1.1) and thereby describe a composition-dependent heat of mixing [28, 29]. However, their formulation is replete with phenomenological parameters with only a vague molecular basis [27].

In order to rectify some of the above deficiencies, Flory developed what is now called the equation of state theory for the statistical thermodynamic properties of polymer systems [24, 30, 31]. The approach combines statistical mechanical models with thermodynamic phenomenology: It utilizes the combinatorial entropy of mixing in Eq. (1.1) and a simple one-dimensional statistical mechanical model to describe the entropic contribution from free volume in perhaps a more realistic form than that provided by introducing voids into the standard lattice model. However, equation of state theories are still forced to introduce a phenomenological parameter corresponding to the entropic contribution to the interaction energy parameter χ, a contribution of completely uncertain molecular origins. Composition dependences in heats and entropies of mixing are modeled by Flory following the work of Prigogine and co-workers [32] by considering polymers to interact through those parts of the molecule that lie on the vaguely defined "surface" of the randomly shaped polymer. However, the relevant surface fractions are incalculable, so they are relegated to additional phenomenological parameters. Recent analyses [33] show that the introduction of a similar type and number of phenomenological parameters into the mean-field lattice theories leads to roughly comparable and therefore operationally equivalent results.

Our interest lies in developing a systematic theory of polymer melts, blends, concentrated solutions, gels, etc. (we term these systems polymeric fluids) that is capable of explaining the molecular origins of the large observed entropic contribution to the phenomenological interaction parameter χ_{eff} and of explaining the pressure, temperature, molecular weight, and composition dependences of this phenomenological parameter. Central to considering a molecular based theory is the establishment of relations between monomer structure and their interactions with the physical properties of melts, blends, and concentrated polymer solutions. We now briefly digress to mention certain aspects of the theory of polymers in dilute and semidilute solutions to assess whether the lattice model is most likely the source of inadequacy in FH theory.

The standard lattice model of self and mutually avoiding polymers with nearest-neighbor nonbonded van der Waals interactions (Fig. 1) has been widely used in conjunction with Monte Carlo simulations to predict correctly a wide range of subtle properties of dilute and semidilute polymer solutions [34], and simulations are being extended to the more concentrated regimes [35, 36]. The robustness of the lattice model for describing dilute and semidilute polymer solutions suggests that this model should also be of great utility for polymeric fluids and therefore that many deficiencies of Flory–Huggins theory lie with the mean-field approximation of Flory. It is, of course, likely that the transition from the dilute and semidilute solutions to the concentrated limit of polymeric fluids introduces additional physical phenomena that are no longer correctly represented by the lattice model. We note also that analytical theories, which agree both with Monte Carlo simulations and with experiment, are currently available for treating the equilibrium properties of polymers in dilute and semidilute solution [37]. We therefore seek to employ and extend the lattice model to

provide an equally accurate representation of the equilibrium statistical mechanics of polymeric fluids.

The next section summarizes a general scheme for systematically solving the lattice model as well as a generalization of the lattice model in which monomers are given specific molecular structures by allowing them to extend over several lattice sites. The free energy of polymeric fluids is obtained as a cluster expansion in which the Flory–Huggins mean-field approximation is recovered in zero order [38–46]. The cluster expansion is arranged as an expansion in the inverse of the lattice coordination number and in the Mayer f-functions:

$$f_{ij} = \exp(\varepsilon_{ij}) - 1 \tag{1.3}$$

where the ε_{ij} depend on the species occupying sites i and j. Although our original derivation [38–46] of this cluster expansion employs mathematical methods of field theory and particle physics [47–49], several results [46] deduced from those field theoretic methods enable us to present a rather simple algebraic derivation [50–53] of the cluster expansion that does not necessitate the use of field theory.

Section 2 provides the simple algebraic derivation of the cluster expansion for evaluating the lattice model free energy of a compressible binary polymer blend. The derivation is given for the simple case of flexible linear polymers, but previous papers discuss the generalization of this model to polymers in which the monomers are taken to have internal structures and therefore to occupy several lattice sites [43–45]. Such a generalization is important in modelling the properties of real polymers for which the monomers, the solvent molecules, and voids generally have different sizes and shapes. Section 3 presents new results computed for the extrapolated zero angle neutron scattering effective interaction parameter χ_{eff} of binary polymer blends. Paper II discusses [53] the monomer structure, pressure, and composition dependence of χ_{eff} for low polymer molecular weights, where the resultant molecular weight dependence may be useful in extracting the microscopic interaction parameters ε_{ij} from experimental data. On the other hand, Sect. 3 focuses upon the high molecular weight limit in which χ_{eff} becomes independent of the M_i. As we vary monomer structures and the microscopic energy parameters, the large M_i limiting χ_{eff} is found to display several characteristic shapes as a function of composition, in general accord with observations. We also consider the typical temperature dependences of χ_{eff} and their variation with composition and monomer structures. Interest also centers on the behavior of the high molecular weight limit of quasi-athermal blends in which χ_{eff} is insensitive to temperature.

Section 4 analyzes the phase diagrams of compressible polymer blends by studying how cloud point curves depend on microscopic interactions, monomer structures, and molecular weights. Interaction parameters ε_{ij} and monomer structures, determined in paper III by fitting [54] data for χ_{eff}, ΔH^{mix}, and ΔV^{mix} of PS(D)/PVME blends, are used to compute the cloud points for this system. The computations have no additional adjustable parameters and are in good agreement with the experiments of Han et al. [55]. Miscible compressible blends (with $\chi_{12}^{FH} < 0$) yield lower critical solution temperatures that vary considerably with monomer structures, microscopic interaction energies, and molecular weights. More interesting behaviors arise for net repulsive interactions (with $\chi_{12}^{FH} > 0$), where closed loop phase diagrams may appear and where there may be both lower and upper critical solution temperatures. However more work is

necessary to determine how systems must be chosen in order that both critical temperatures lie in the accessible range between the glass transition and thermal decomposition temperatures. Those readers most interested in the applications may skip directly to Sect. 3.

2. Lattice cluster theory of compressible binary polymer blends

This section briefly describes the lattice model and our method for its systematic solution. To maintain simplicity of presentation, we describe the theory for binary blends of linear chains. The application in Sects. 3 and 4, however, considers polymer chains that are composed of structured monomers.

2.1. Model of binary polymer blends

The standard lattice model of a binary polymer blend depicts the two species of polymer chains as sets of N_1 and N_2 identical monomers lying at the lattice sites of a regular array and joined, respectively, by N_1-1 and N_2-1 sequential flexible bonds. Excluded volume constraints prohibit any two monomers from occupying the same lattice site. The lattice structure determines the possible conformations for the n_1 and n_2 polymer chains of species 1 and 2, respectively. n_v unoccupied lattice sites, called voids, model the free volume with void volume fraction $\phi_v = n_v/N_l$. While the lattice model of monatomic fluids is a rather poor representation of reality, mostly because voids and molecules are taken as having the same size, lattice models of polymeric fluids, which do not suffer from this problem, are likely to be better. Although, there is no limitation on introducing arbitrary lattices, we consider only hypercubic lattices with coordination number $z = 2d$, where d is the dimensionality.

The extended lattice model permits monomers of a given species to cover $s_\alpha > 1$ lattice sites, so each chain occupies $M_\alpha = N_\alpha s_\alpha$ sites. This extension allows us to distinguish between different polymer architectures and to investigate the influence of monomer molecular structure on the thermodynamic properties of blends. The structured monomers of polymer species α and β interact with nearest neighbor attractive van der Waals energies $\varepsilon_{\alpha\beta}$. Since all monomer portions are taken, for simplicity, as energetically equivalent, there are only three independent energies ε_{11}, ε_{22}, and ε_{12}. These microscopic energies, together with temperature, molecular weights, and blend composition [as represented by the volume fractions $\phi_i = n_i N_i s_i/N_l$, (satisfying $\phi_1 + \phi_2 + \phi_v = 1$) or by the composition variables $\Phi_1 = 1 - \Phi_2 = n_1 N_1 s_1/(n_1 N_1 s_1 + n_2 N_2 s_2)$] are input parameters in the lattice cluster theory (LCT).

The position of the ith lattice site (with respect to the origin of coordinates) is designated by the vector $\boldsymbol{r}_i$. Two lattice sites i and j are nearest neighbors when their positions $\boldsymbol{r}_i$ and $\boldsymbol{r}_j$ are related to each other by:

$$\boldsymbol{r}_i = \boldsymbol{r}_j + \boldsymbol{a}_\beta, \tag{2.1}$$

where the $\boldsymbol{a}_\beta$ ($\beta = 1, \ldots, z$) are the vectors from the lattice site i to its z possible nearest neighbors. It is useful to represent a nearest neighbor constraint from Eq. (2.1) by using the Kronecker delta function:

$$\delta(i, j + \beta) \equiv \delta(\boldsymbol{r}_i, \boldsymbol{r}_j + \boldsymbol{a}_\beta). \tag{2.2}$$

2.2. *Packing entropy in the athermal limit for blends of linear polymer chains*

2.2.1. Analytical representation of the lattice model. The system contains n_1 and n_2 monodisperse linear polymer chains with polymerization indices N_1 and N_2 for polymer species 1 and 2, respectively. The polymer chain conformations are described in the lattice model by specifying sequences of monomer locations at lattice sites. The athermal limit packing partition function involves the sum over all possible configurations of the $n_p = n_1 + n_2$ polymer chains and can be written exactly with the aid of Eq. (2.2) as:

$$W(n_1, n_2, N_1, N_2) = \prod_{\mu=1}^{2} \frac{1}{n_\mu! 2^{n_\mu}} \sum_{\substack{i^1_{1,1} \neq i^1_{2,1} \neq \cdots \neq i^1_{N_1,1} \\ \neq i^1_{1,2} \neq i^1_{2,2} \neq \cdots \neq i^1_{N_1,2} \\ \cdots\cdots\cdots\cdots \\ \neq i^1_{1,n_1} \neq i^1_{2,n_1} \neq \cdots \neq i^1_{N_1,n_1} \\ \cdots\cdots\cdots\cdots \\ \neq i^2_{1,n_2} \neq i^2_{2,n_2} \neq \cdots \neq i^2_{N_2,n_2}}} \times \prod_{m_\mu=1}^{n_\mu} \left\{ \prod_{\alpha_\mu=1}^{N_\mu - 1} \sum_{\beta^\mu_{\alpha,m}=1}^{z} \delta(i^\mu_{\alpha,m}, i^\mu_{\alpha+1,m} + \beta^\mu_{\alpha,m}) \right\}. \quad (2.3)$$

The first bond on the first chain of species 1 enters into Eq. (2.3) with the factor of $\sum_{i^1_{1,1}, i^1_{2,1}} \sum_{\beta^1_{1,1}} \delta(i^1_{1,1}, i^1_{2,1} + \beta^1_{1,1})$, where the superscript labels the species (1 or 2), the first subscript indicates the sequential monomer numbering along the chain, and the second subscript specifies the chain number of a given species. The next bond in this chain contributes to the partition function a factor of $\sum_{i^1_{3,1}} \sum_{\beta^1_{2,1}} \delta(i^1_{2,1}, i^1_{3,1} + \beta^1_{2,1})$ with the obvious excluded volume constraint between the nonbonded first and third monomers $i^1_{3,1} \neq i^1_{1,1}$, etc. This process is continued for all bonds and all chains. A factor $1/(n_\mu! 2^{n_\mu})$ for each component $\mu = 1, 2$ accounts for chain indistinguishability and for the identity of chain ends. The excluded volume constraint $i^1_{1,1} \neq \cdots \neq i^2_{N_2,n_2}$ prohibits any two monomers in the system from occupying the same lattice site. This constraint in the summation of Eq. (2.3) is also applied to bonded monomers only for notational symmetry since the Kronecker deltas in Eq. (2.3) automatically produce vanishing contributions from unphysical one-bond loops [52].

2.2.2. Flory mean field approximation. The exact representation of Eq. (2.3) of the lattice model enables us to extract the mean field Flory–Huggins approximation as zeroth order and to expand the remainder in terms of contributions generated by successively larger scale correlations. In order to derive this expansion, each of the Kronecker deltas in Eq. (2.3) is first replaced by its lattice Fourier transform:

$$\delta(i, j + \beta) = N_l^{-1} \sum_{\boldsymbol{q}} \exp[i\boldsymbol{q} \cdot (\boldsymbol{r}_i - \boldsymbol{r}_j - \boldsymbol{a}_\beta)], \quad (2.4)$$

where N_l is the total number of lattice sites and the wave vector summations index $\boldsymbol{q}$ runs over the first Brillouin zone. Summation of $\delta(i, j + \beta)$ in Eq. (2.4) over all bond directions $\beta = 1, \ldots, z$ and rearrangement produce:

$$\sum_{\beta} \delta(i, j + \beta) = \frac{z}{N_l} \left\{ 1 + \frac{1}{z} \sum_{\boldsymbol{q} \neq 0} f(\boldsymbol{q}) \exp[i\boldsymbol{q} \cdot (\boldsymbol{r}_i - \boldsymbol{r}_j)] \right\}, \quad (2.5)$$

where the $\boldsymbol{q} = 0$ term has been conveniently separated and where the nearest neighbor structure factor is:

$$f(\boldsymbol{q}) = \sum_{\beta=1}^{z} \exp(-i\boldsymbol{q} \cdot \boldsymbol{a}_\beta). \tag{2.6}$$

Equation (2.5) is now substituted into Eq. (2.3) for each Kronecker delta. Thus, each bond, labelled by the three indices α, m, and μ, introduces the "momentum" vector $\boldsymbol{q}^{\mu}_{\alpha,m}$. The packing partition function of Eq. (2.3) is then transformed exactly into:

$$W = \prod_{\mu=1}^{2} \frac{1}{n_\mu! 2^{n_\mu}} \sum_{i^1_{1,1} \neq \cdots \neq i^2_{N_2,n_2}} \prod_{m_\mu=1}^{n_\mu} \prod_{\alpha_\mu=1}^{N_\mu - 1} \left[\frac{z}{N_l}\right]$$

$$\times \left\{1 + \frac{1}{z} \sum_{\boldsymbol{q}^{\mu}_{\alpha,m} \neq 0} f(\boldsymbol{q}^{\mu}_{\alpha,m}) \exp[i\boldsymbol{q}^{\mu}_{\alpha,m} \cdot (\boldsymbol{r}_{i^{\mu}_{\alpha,m}} - \boldsymbol{r}_{i^{\mu}_{\alpha+1,m}})]\right\}. \tag{2.7}$$

When a single bond correlation correction is defined as:

$$X^{\mu}_{\alpha,m} \equiv \frac{1}{z} \sum_{\boldsymbol{q}^{\mu}_{\alpha,m} \neq 0} f(\boldsymbol{q}^{\mu}_{\alpha,m}) \exp[i\boldsymbol{q}^{\mu}_{\alpha,m} \cdot (\boldsymbol{r}_{i^{\mu}_{\alpha,m}} - \boldsymbol{r}_{i^{\mu}_{\alpha+1,m}})] \tag{2.8}$$

and is inserted into Eq. (2.7), the resulting expression:

$$W(n_1, n_2, N_1, N_2) = \prod_{\mu=1}^{2} \frac{1}{n_\mu! 2^{n_\mu}} \sum_{i^1_{1,1} \neq \cdots \neq i^2_{N_2,n_2}} \prod_{m_\mu=1}^{n_\mu} \prod_{\alpha_\mu=1}^{N_\mu - 1} \left\{\left[\frac{z}{N_l}\right][1 + X^{\mu}_{\alpha,m}]\right\}, \tag{2.9}$$

is shown below to exhibit the form of a cluster expansion that bears a strong similarity to the virial series of Mayer. The totally uncorrelated contribution in Eq. (2.9) arises from the factors of unity in braces [the $\boldsymbol{q} = 0$ terms in Eq. (2.5)] from *all bonds* and yields the Flory–Huggins mean field approximation:

$$W^{MF}(n_1, n_2, N_1, N_2) = \prod_{\mu=1}^{2} \frac{1}{n_\mu! 2^{n_\mu}} \sum_{i^1_{1,1} \neq \cdots \neq i^2_{N_2,n_2}} \prod_{m_\mu=1}^{n_\mu} \prod_{\alpha_\mu=1}^{N_\mu - 1} \left[\frac{z}{N_l}\right]. \tag{2.10}$$

Carrying out the summation and products simplifies Eq. (2.10) to:

$$W^{MF}(n_1, n_2, N_1, N_2) = \prod_{\mu=1}^{2} \frac{1}{n_\mu! 2^{n_\mu}} \frac{N_l!}{\left(N_l - \sum_{\mu=1}^{k} N_\mu n_\mu\right)!} \left[\frac{z}{N_l}\right]^{\sum_{\mu=1}^{2} n_\mu (N_\mu - 1)}, \tag{2.11}$$

which may be shown to recover the classic Flory–Huggins combinatorial packing entropy of mixing [1] (with self-reversal included) for a binary compressible polymer blend. Corrections to the mean field partition function W^{MF} are discussed below.

2.2.3. Cluster expansion for corrections to the Flory–Huggins packing entropy. The quantity $X^{\mu}_{\alpha,m}$ of Eq. (2.8) depends on the positions of the two segments forming the αth bond on the mth chain of polymer species μ. These $X^{\mu}_{\alpha,m}$ produce the corrections [to the Flory–Huggins approximation of Eq.

(2.11)] as arising from correlations in monomer positions. Expanding the product in Eq. (2.9) naturally generates the cluster expansion:

$$\prod_{m_\mu=1}^{n_\mu}\prod_{\alpha_\mu=1}^{N_\mu-1}[1+X^{\mu}_{\alpha,m}]=1+\sum_{\mu,\alpha_\mu,m_\mu}X^{\mu}_{\alpha,m}+\sum_{(\mu,\alpha_\mu,m_\mu)>(\mu',\alpha'_{\mu'},m'_{\mu'})}X^{\mu}_{\alpha,m}X^{\mu'}_{\alpha',m'}+\cdots, \tag{2.12}$$

where the notation $(\mu, \alpha_\mu, m_\mu) > (\mu', \alpha'_{\mu'}, m'_{\mu'})$ indicates that the summation in Eq. (2.12) runs over all distinct pairs of bonds in the system. When Eq. (2.12) is substituted into Eq. (2.9), the linear terms in $X^{\mu}_{\alpha,m}$ from Eq. (2.12) emerge as one-correlating bond contributions, the quadratic terms as two-correlating bond, etc., contributions. Thus, the packing entropy partition function may be written as:

$$W(n_1,n_2,N_1,N_2)=W^{MF}(n_1,n_2,N_1,N_2)\times\left\{1+\frac{\left(N_l-\sum_{\mu=1}^{2}n_\mu N_\mu\right)!}{N_l!}\sum_{i^1_{1,1}\neq\cdots\neq i^2_{N_2,n_2}}\left[\sum_{\mu,\alpha_\mu,m_\mu}X^{\mu}_{\alpha,m}+\sum_{(\mu,\alpha_\mu,m_\mu)>(\mu',\alpha'_{\mu'},m'_{\mu'})}X^{\mu}_{\alpha,m}X^{\mu'}_{\alpha',m'}+\cdots\right]\right\}. \tag{2.13}$$

Performing all summations in Eq. (2.13) leads to the more compact form:

$$W(n_1,n_2,N_1,N_2)=W^{MF}(n_1,n_2,N_1,N_2)\left[1+\sum_B\gamma_D(n_1,n_2,N_1,N_2)D_B\right], \tag{2.14}$$

where the summation in Eq. (2.14) may be represented diagrammatically as described by Nemirovsky et al. [42] for the original field theory formulation. The value of a given diagram with B correlating bonds is the product of a monomer structure independent connectivity constant D_B and a monomer structure dependent combinatorial factor γ_D. (See papers I, II, and references therein for more details.) The sum over B in Eq. (2.14) is understood to designate both a sum over all diagrams with B bonds and a sum over B.

Athermal limit packing entropies follow simply from the Boltzmann definition:

$$\begin{aligned}S(n_1,n_2,N_1,N_2)&=k\ln W(n_1,n_2,N_1,N_2)\\&=k\ln W^{MF}(n_1,n_2,N_1,N_2)+k\ln\left[1+\sum_B\gamma_D(n_1,n_2,N_1,N_2)D_B\right].\end{aligned} \tag{2.15}$$

Expansion of the logarithm in the right-most term in Eq. (2.14) and formation of cumulants serve to cancel exactly the unphysical (hyper-extensive) contributions from individual diagrams in Eq. (2.14). After some rearrangement, the final expression:

$$S(n_1,n_2,N_1,N_2)=k\ln W^{MF}(n_1,n_2,N_1,N_2)+k\sum_B[\gamma_D(n_1,n_2,N_1,N_2)D_B]^{(c)} \tag{2.16}$$

provides the noncombinatorial portion of $S(n_1, n_2, N_1, N_2)$ as a sum of the contributions from cumulant cluster diagrams $[\gamma_D(n_1, n_2, N_1, N_2)D_B]^{(c)}$ that are described more fully in Ref. [52].

2.3. Helmholtz free energy for nonathermal blends

2.3.1. Partition function for interacting binary polymer blends. The lattice model of polymer fluids contains both short range repulsions and longer range attractions. The former are described by the excluded volume constraints prohibiting any two monomers from lying at the same lattice site, while the attractive interactions are introduced by ascribing a van der Waals attractive energy $\varepsilon^{ij}_{\mu\lambda}$ to each pair of species μ and λ monomers that occupy nearest neighbor lattice sites i and j (as in Fig. 1). The partition function $Z(n_1, n_2, N_1, N_2)$ for the interacting system, therefore, must include the Boltzmann factor:

$$\exp\left[\sum_{\mu=1}^{2}\sum_{\lambda\leqslant\mu}\sum_{\substack{i\in S_\mu\\ j\in S_\lambda}}{}' \varepsilon^{ij}_{\mu\lambda}\right], \tag{2.17}$$

where S_μ designates the set of lattice sites occupied by polymer segments of species μ, etc. All energies $\varepsilon_{\mu\lambda}$ in Eq. (2.17) are expressed in units of k_BT, and the prime on the sum in (2.17) implies the constraint that when $\mu = \lambda$, we require $j \leqslant i$.

The total configurational partition function $Z(n_1, n_2, N_1, N_2)$ is obtained by inserting Eq. (2.17) into the summand on the right-hand side of Eq. (2.3) as:

$$Z(n_1, n_2, N_1, N_2) = \prod_{\mu=1}^{2}\frac{1}{n_\mu!2^{n_\mu}}\sum_{i^1_{1,1}\neq\cdots\neq i^2_{N_2,n_2}}\prod_{m_\mu=1}^{n_\mu}\prod_{\alpha_\mu=1}^{N_\mu-1}\sum_{\beta^\mu_{\alpha,m}=1}^{z}\delta(i^\mu_{\alpha,m}, i^\mu_{\alpha+1,m}+\beta^\mu_{\alpha,m})$$
$$\times\exp\left[\sum_{\mu=1}^{2}\sum_{\lambda\leqslant\mu}\sum_{\substack{i\in S_\mu\\ j\in S_\lambda}}{}' \varepsilon^{ij}_{\mu\lambda}\right]. \tag{2.18}$$

The S_μ in the summation represents the set of occupied lattice sites $i^\mu_{1,1}\neq\cdots\neq i^\mu_{N_\mu,n_\mu}$, and this ties the summation indices i and j in the van der Waals energy factor to those in the outer summation emerging from Eq. (2.3). Thus, i and j in Eq. (2.18) run over all pairs of lattice sites that are occupied by monomers of species μ and λ, respectively.

2.3.2. Mayer-like Cluster expansion for attractive interactions. The Boltzmann factor in Eq. (2.17) may be rewritten in terms of Mayer f-functions:

$$f_{\mu\lambda} = \exp(\varepsilon_{\mu\lambda}) - 1 \tag{2.19}$$

as the product form:

$$\exp\left[\sum_{\mu=1}^{2}\sum_{\lambda\leqslant\mu}\sum_{\substack{i\in S_\mu\\ j\in S_\lambda}}{}' \varepsilon^{ij}_{\mu\lambda}\right] = \prod_{\mu=1}^{2}\prod_{\lambda\leqslant\mu}\prod_{\substack{i\in S_\mu\\ j\in S_\lambda}}{}'\left[1+\sum_{\beta=1}^{z}\delta(i, j+\beta)f_{\mu\lambda}\right], \tag{2.20}$$

where the prime on the product has the same meaning as that on the sum in Eq. (2.17) and the Kronecker delta arises from the nearest neighbor character of the attractive interactions. Expanding the product of Eq. (2.20) in the usual Mayer fashion yields the cluster expansion:

$$\prod_{\mu=1}^{2}\prod_{\lambda\leqslant\mu}\prod_{\substack{i\in S_\mu\\ j\in S_\lambda}}{}'\left[1+\sum_{\beta=1}^{z}\delta(i,j+\beta)f_{\mu\lambda}\right]=1+\sum_{\mu=1}^{2}\sum_{\lambda\leqslant\mu}\sum_{\beta=1}^{z}\sum_{i\geqslant j}\delta(i,j+\beta)f_{\mu\lambda}$$

$$+\sum_{\mu,\mu'=1}^{2}\sum_{\substack{\lambda\leqslant\mu\\ \lambda'\leqslant\mu'}}\sum_{\beta,\beta'=1}^{z}\sum_{(i\geqslant j)\neq(i'\geqslant j')}\delta(i,j+\beta)\delta(i',j'+\beta')f_{\mu\lambda}f_{\mu'\lambda'}+\cdots. \tag{2.21}$$

The right side of Eq. (2.21) along with identity Eq. (2.4) for each $\delta(i,j+\beta)$ is inserted into Eq. (2.18) to generate a double cluster expansion for the partition function $Z(n_1,n_2,N_1,N_2)$. When this is done, the $\boldsymbol{q}=0$ terms in the energetic contribution to $Z(n_1,n_2,N_1,N_2)$ of Eq. (2.21) may be separated into two categories. Those contributions remaining in the thermodynamic limit provide the leading Flory–Huggins interaction energy and a simple renormalization of the Mayer f-functions as described in Appendix A of Ref. [52]. The evaluation of the remaining $\boldsymbol{q}\neq 0$ contributions from the combination of Eq. (2.5) and the expansion of Eq. (2.21) then proceeds almost identically to that for the packing entropies in Eqs. (2.13)–(2.16) [52].

The Helmholtz free energy $F(n_1,n_2,N_1,N_2)$ is thus obtained from the partition function $Z(n_1,n_2,N_1,N_2)$ through:

$$F(n_1,n_2,N_1,N_2)=-k_BT\ln Z(n_1,n_2,N_1,N_2). \tag{2.22}$$

The diagrammatic representation of Eq. (2.22) may be represented symbolically as:

$$-\frac{F(n_1,n_2,N_1,N_2)}{k_BT}=\ln W^{MF}(n_1,n_2,N_1,N_2)+N_l\frac{z}{2}\sum_{\mu=1}^{2}\sum_{\lambda=1}^{2}f_{\mu\lambda}\phi_\mu\phi_\lambda$$

$$+\ln\left\{1+\sum_{B,l}\gamma_{D,l}(n_1,n_2,N_1,N_2)D_{B,l}\right\}, \tag{2.23}$$

where $W^{MF}(n_1,n_2,N_1,N_2)$ and $f_{\mu\lambda}$ are given by Eqs. (2.11) and (2.19), respectively, and where the quantities $D_{B,l}$ and $\gamma_{D,l}$ are generalizations of the D_B and γ_D of Sect. 2 to a new class of diagrams that contain l f-bond interaction lines in addition to B correlating bonds. The sum over B and l in Eq. (2.23) denotes both a sum over all different diagrams with B bonds and l f-function interaction lines and a sum over B and l, excluding only $B=l=0$. The diagrams and their evaluation are described in detail by paper I and references therein.

The standard procedure of expressing the Helmholtz free energy $F(n_1,n_2,N_1,N_2)$ as a direct sum of diagrammatic contributions employs the expansion of each Mayer f-function $f_{\mu\lambda}$ in Eq. (2.23) as a power series in $\varepsilon_{\mu\lambda}$ and the subsequent expansion of the last logarithm in Eq. (2.23) as a Taylor series. Collecting the resulting contributions with a given power of $\varepsilon_{\mu\lambda}$ into cumulants ensures the exact cancellation of higher order terms in N_l. The free energy is then written in the form:

$$-\frac{F(n_1,n_2,N_1,N_2)}{k_BT}=\ln W^{MF}(n_1,n_2,N_1,N_2)+N_l\frac{z}{2}\sum_{\mu=1}^{2}\sum_{\lambda=1}^{2}\varepsilon_{\mu\lambda}\phi_\mu\phi_\lambda$$

$$+\sum_{B,l}[\gamma_{D,l}(n_1,n_2,N_1,N_2)D_{B,l}]^{(c)}, \tag{2.24}$$

where $[\gamma_{D,l}(n_1,n_2,N_1,N_2)D_{B,l}]^{(c)}$ are the generalized cumulant cluster diagrams of Ref. [52] which reduce for $l=0$ to the cumulant cluster diagrams in Eq. (2.16).

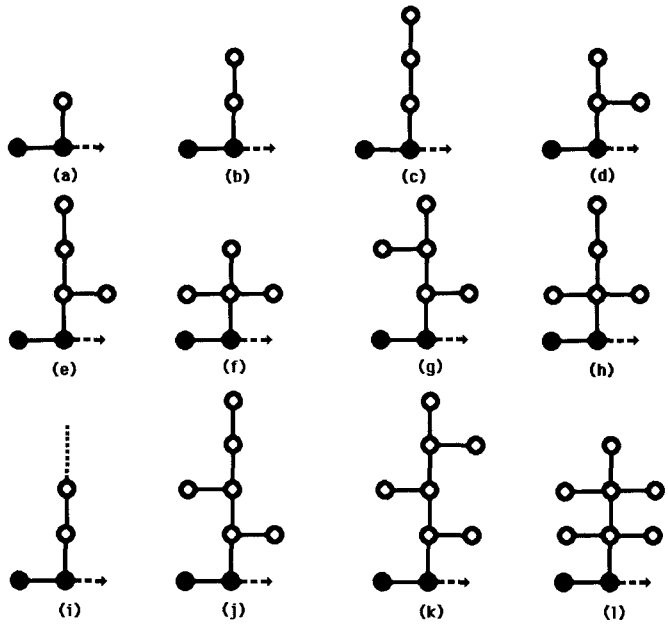

Fig. 2. Examples of vinyl monomer structures that extend over $s_\alpha > 1$ neighboring lattice sites. Polymer chains are constructed by linking backbone submonomer units (solid circles) in the direction of the arrows. All bonds including those joining side groups (open circles) are fully flexible in three dimensions

The sum of the generalized cumulant cluster diagrams provides all corrections to FH, while the two first terms of the right hand side of Eq. (2.24) are the $\boldsymbol{q} = 0$ limit FH athermal entropic and energetic contributions, respectively.

3. Small angle neutron scattering effective interaction parameter χ_{eff} for binary compressible blends

Although the algebraic derivation of the LCT for the athermal limit packing entropy in Eq. (2.16) and for the Helmholtz free energy of Eq. (2.24) of binary compressible polymer blends is presented in Sect. 2 for linear chains, the final expression of Eqs. (2.16) and (2.24) are quite general and apply to polymers with structured monomers, provided that the diagrams and factors $\gamma_{D,l}$ are suitably generalized as described [52] in paper I. Figure 2 displays some examples of the vinyl monomer structures that are considered here. Chains of species α have polymerization indices N_α and monomers that occupy s_α sites. The total number of sites occupied by a chain of species α, the site occupancy index M_α, is thus $M_\alpha = N_\alpha s_\alpha$. The composition of these structured monomer blends may be expressed in terms of volume fractions $\phi_\alpha = n_\alpha M_\alpha / N_l$, nominal volume fractions $\Phi_\alpha \equiv \phi_\alpha/(1-\phi_v)$ or experimental volume fractions that are defined in terms of pure α melt volumes V_α as $\phi_\alpha^{(exp)} \equiv V_\alpha/(V_1 + V_2)$.

3.1. Binary blend at constant pressure

After extending the theory to chains with structured monomers and after computing and rearranging separate cumulant diagram contributions to the LCT

Helmholtz free energy of mixing, Eq. (2.24) becomes a polynomial in the volume fractions ϕ_α and ϕ_v with the general structure:

$$\frac{\Delta F^{mix}}{N_l k_B T} = \phi_v \ln \phi_v + \frac{\phi_1}{M_1} \ln \phi_1 + \frac{\phi_2}{M_2} \ln \phi_2 + \phi_1 \phi_2 \sum_{\substack{i,j=0 \\ i+j \leqslant 4}} g_{12}^{(i,j)} \phi_1^i \phi_v^j + \phi_1 \phi_v \sum_{\substack{i,j=0 \\ i+2j \leqslant 6}} g_{1v}^{(i,j)} \phi_1^i \phi_v^j + \phi_2 \phi_v \sum_{\substack{i,j=0 \\ i+2j \leqslant 6}} g_{2v}^{(i,j)} \phi_2^i \phi_v^j, \tag{3.1}$$

where logarithmic terms provide the traditional FH combinatorial entropy of mixing for a compressible blend and where the upper limits on the summations arise because of the approximations used [52]. The coefficients $g_{12}^{(i,j)}$, $g_{1v}^{(i,j)}$, and $g_{2v}^{(i,j)}$ in Eq. (3.1) are expanded in the inverse coordination number $1/z$ and in the three microscopic interaction energies ε_{11}, ε_{22}, and ε_{12} (in units of $k_B T$). Using symbolic notation, this double series is expressed as:

$$g_{\alpha\beta}^{(i,j)} = \sum_{q,r} (z)^{-q} (\varepsilon_{\alpha\beta})^r C_{p,q}^{(i,j)}, \quad (\alpha \neq \beta) \tag{3.2}$$

where, for instance, terms in $(\varepsilon_{\alpha\beta})^2$ represent quadratic contributions like $\varepsilon_{11}^2, \varepsilon_{11}\varepsilon_{12}, \varepsilon_{11}\varepsilon_{22}$, etc. and $\varepsilon_{\alpha v} \equiv \varepsilon_{\alpha\alpha}$. The coefficients $C_{p,q}^{(i,j)}$ in Eq. (3.2) are functions of the site occupancy indices M_α and the monomer structure dependent combinatorial factors $N_i^{(\alpha)}, N_{i,j}^{(\alpha)}, \ldots$ that are defined in detail and are tabulated [54] in paper III.

While the Helmholtz free energy F in Eq. (3.1) describes the thermodynamic properties of a polymer blend at constant volume V, the Gibbs free energy $G = F + PV$ is designed for systems at constant pressure P. Converting the free energy of mixing ΔF^{mix} into:

$$\Delta G^{mix} = \Delta F^{mix} + P \, \Delta V^{mix} \tag{3.3}$$

requires specification of the pressure and the computation of the volume change on mixing. The former is evaluated from the Helmholtz free energy of Eq. (3.1) as:

$$P = -\left.\frac{\partial \Delta F^{mix}}{\partial V}\right|_{T,n_1,n_2} = \left[-\ln \phi_v - (1-\phi_v) + \frac{\phi_1}{M_1} + \frac{\phi_2}{M_2} + \phi_1\phi_2 p_{12} + \phi_1 \phi_v p_{1v} + \phi_2 \phi_v p_{2v} \right] (k_B T)/a^3 \tag{3.4}$$

with

$$p_{12} \equiv \sum_{\substack{i,j=0 \\ i+j \leqslant 4}} g_{12}^{(i,j)} \phi_1^i \phi_v^{j-1} [(i+j+1)\phi_v - j], \tag{3.4a}$$

$$p_{\alpha v} \equiv \sum_{\substack{i,j=0 \\ i+2j \leqslant 6}} g_{\alpha v}^{(i,j)} \phi_\alpha^i \phi_v^{j-1} [(i+j+1)\phi_v - (j+1)], \quad \alpha = 1, 2, \tag{3.4b}$$

where a is the lattice constant that is assumed here to be temperature independent. Equation (3.4) enables the numerical determination of the void volume fraction ϕ_v as a function of P, M_1, M_2, T, and a for arbitrary blend compositions Φ_1. Analogous equations of state can be derived for pure melts from the free energy of mixing ΔF_α^{mix} that is obtained from Eq. (3.1) by setting $\phi_\beta = 0$ $(\beta \neq \alpha)$.

The pressure $P^{(\alpha)}$ of a pure melt α thus emerges from the melt analogue of Eq. (3.1) as:

$$P^{(\alpha)} = -\frac{\partial \Delta F_{\alpha}^{mix}}{\partial V}\bigg|_{T,n_\alpha} = \Bigg[-\ln \phi_v^{(\alpha)} - (1-\phi_v^{(\alpha)}) + \frac{(1-\phi_v^{(\alpha)})}{M_\alpha} + \phi_v^{(\alpha)}(1-\phi_v^{(\alpha)}) p_{\alpha v} \Bigg] k_B T/a^3, \quad (3.5)$$

where $p_{\alpha v}$ is given by Eq. (3.4b) with $\phi_v = \phi_v^{(\alpha)}$ and $\phi_\alpha = (1-\phi_v^{(\alpha)})$ and where $\phi_v^{(\alpha)}$ denotes the void volume fraction in the compressible melt of pure component α. The latter also determines the volume of mixing:

$$\Delta V^{mix} = V - V_1 - V_2 = V\left(1 - \frac{\phi_1}{(1-\phi_v^{(1)})} - \frac{\phi_2}{(1-\phi_v^{(2)})}\right) \quad (3.6)$$

and therefore by Eq. (3.3) provides ΔG^{mix}. We numerically invert Eqs. (3.4) and (3.5) to obtain $\phi_v = \phi_v[n_1, n_2, n_v(n_1, n_2, P, T)]$ and $\phi_v^{(\alpha)} = \phi_v^{(\alpha)}(P, T)$ for insertion into Eqs. (3.3)–(3.6). Since the thermodynamic quantities are defined for a stable homogeneous one-phase blend, stability must be checked for each set of M_α, P, T, Φ_1, and a used in computations. A binary polymer blend at constant temperature T and pressure P has only one stability condition:

$$\frac{\partial^2 G}{\partial \Phi_1^2}\bigg|_{P,T} > 0. \quad (3.7)$$

The derivatives in Eq. (3.7) are readily evaluated numerically.

3.2. Definitions of small angle neutron scattering effective interaction parameter χ_{eff}

The effective site-site Flory interaction parameter χ_{eff} is often defined (using the incompressible random phase approximation) in terms of the extrapolated zero angle neutron scattering function $S(0)^{-1}$ as:

$$\chi_{eff} = -\frac{1}{2}\left[S(0)^{-1} - \frac{1}{M_1\Phi_1} - \frac{1}{M_2\Phi_2}\right]. \quad (3.8)$$

The blend composition variables in Eq. (3.8) are nominal volume fractions Φ_i that satisfy the condition $\Phi_1 + \Phi_2 = 1$ and that are connected with the volume fractions ϕ_i by $\Phi_i = \phi_i/(1-\phi_v)$. A slightly modified definition of χ_{eff}:

$$\chi'_{eff} = -\frac{1}{2}\left[S(0)^{-1} - \frac{1}{M_1\phi_1^{(exp)}} - \frac{1}{M_2\phi_2^{(exp)}}\right] \quad (3.8a)$$

contains the experimental volume fraction $\phi_\alpha^{(exp)}$ instead of Φ_α. However, the differences between χ_{eff} and χ'_{eff} of Eqs. (3.8) and (3.8a), respectively, are rather small and vanish in the long chain limit of $M_1, M_2 \to \infty$. The total (observed) extrapolated zero angle structure factor $S(0)$ is a weighted sum of the zero wave vector partial structure factors $S_{\alpha\beta}(0)$:

$$S(0) = p_1^2 S_{11}(0) + 2p_1 p_2 S_{12}(0) + p_2^2 S_{22}(0), \quad (3.9)$$

where the weights p_1 and p_2 are reduced scattering lengths that are normalized such that $p_1 - p_2 = 1$. When the scattering contrast is complete and the scattering is by monomers of species 1, the reduced scattering length of species 2 becomes

$p_2 = 0$, and Eq. (3.9) yields $S(0) = S_{11}(0)$. The zero wave vector partial structure factors $S_{\alpha\beta}(0)$ are related to the chemical potentials μ_α and μ_β by:

$$S_{\alpha\beta}(0)^{-1} = \frac{N_l}{M_\alpha M_\beta k_B T} \frac{\partial \mu_\alpha}{\partial n_\beta}\bigg|_{T,V,\mu_\beta} . \tag{3.10}$$

Since the chemical potentials μ_1 and μ_2 can be easily evaluated from the free energy of Eq. (3.1), Eqs. (3.8) and (3.10) readily provide the effective interaction parameter χ_{eff}. For simplicity, the calculations presented here just employ the definition of Eq. (3.10) for the perfect scattering contrast assumption, but the general case is readily treated.

Experimental neutron scattering data are sometimes analyzed [55] in terms of a monomer pair interaction parameter χ''_{eff} that is defined by:

$$\frac{\chi''_{eff}}{v_o} = -\frac{1}{2}\left[\frac{S(0)^{-1}}{v_c} - \frac{1}{N_1 v_1 \phi_1^{(exp)}} - \frac{1}{N_2 v_2 \phi_2^{(exp)}}\right]. \tag{3.11}$$

The reference unit cell volume $v_o = (v_1 v_2)^{1/2}$ is the geometrical mean of monomer volumes v_i, and v_c in Eq. (3.11) denotes the cell volume associated with a single lattice site. This χ''_{eff} is related to χ'_{eff} of Eq. (3.8a) through the composition independent factor $(s_1 s_2)^{1/2}$:

$$\chi''_{eff} = \chi'_{eff}(s_1 s_2)^{1/2} \tag{3.12}$$

with s_α being the number of lattice sites occupied by one monomer of species α.

3.3. Dependence of small angle neutron scattering interaction parameter χ_{eff} on molecular weights

Paper II studies [53] some features of the neutron scattering χ_{eff} for binary compressible blends, but the majority of the computations there involve low molecular weights to emphasize the resultant molecular weight dependence that emerges principally for low volume fractions of one of the blend components. This low molecular weight limit is useful in experiments as providing information to determine three independent microscopic interaction energies, but many applications involve high molecular weights. Thus, we consider here the large molecular weight limit and the transition to this limit. As the monomer molecular structure and the microscopic interaction energies are varied, the high molecular weight limiting χ_{eff} is found to exhibit several characteristic shapes with magnitudes dependent on the system and structure parameters. Hence, one of our objectives is to illustrate these general trends.

The polymer molecular weights $M_w^{(\alpha)}$ are proportional to the site occupancy indices M_α as:

$$M_w^{(\alpha)} = M_\alpha M_{mon}^{(\alpha)} / s_\alpha, \tag{3.13}$$

where $M_{mon}^{(\alpha)}$ is the molecular weight of a single monomer. The compressible LCT calculations of Figs. 3–14 for χ_{eff} are performed for the usual experimental pressure of $P = 1$ atm, and they employ a simple cubic lattice with coordination number $z = 6$ and the lattice constant $a = 2.5477$ A.

The influence of molecular weights on χ_{eff} is further illustrated by comparing Figs. 3 and 4, where all else is the same apart from the polymerization indices which are 100 and 10^4, respectively. Component 1 has the monomer structure *a* of Fig. 2, while component 2 has structure *c*. (In the following the component

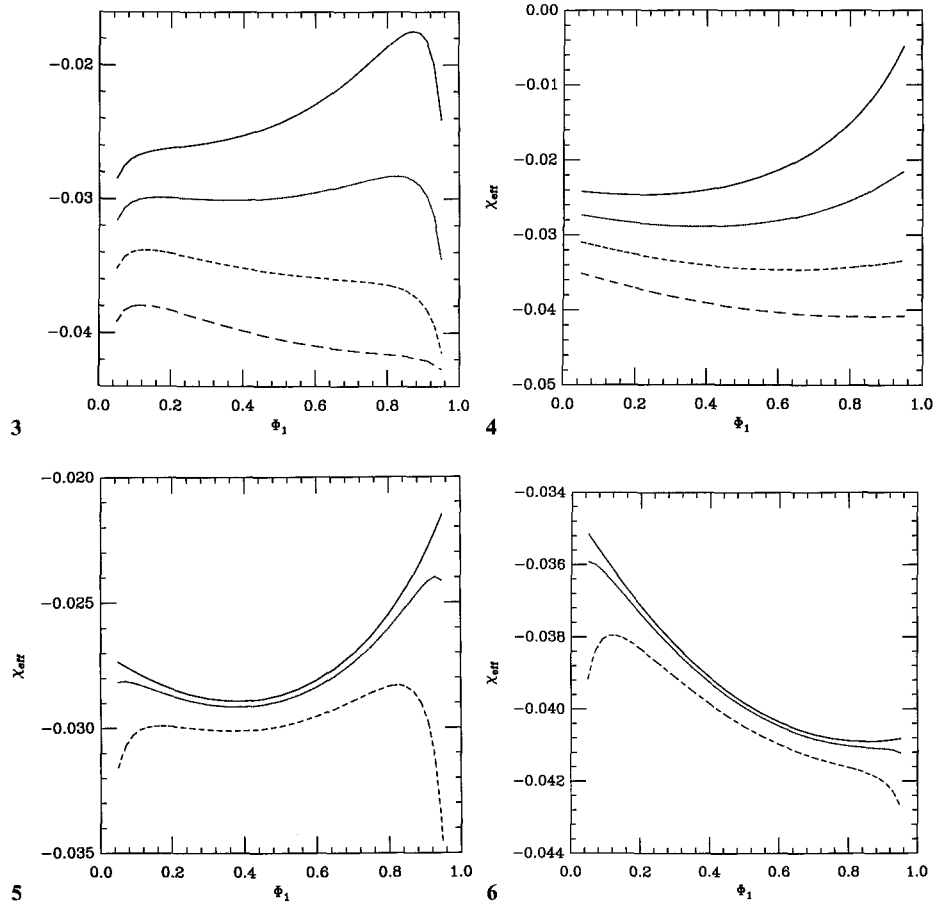

Fig. 3. Low molecular weight LCT small angle neutron scattering effective interaction parameter $\chi_{eff}(\Phi_1)$ of a model $a-c$ binary blend for various self-interaction energies ε_{11} but constant $\varepsilon_{22}/k_BT = 0.6$ and $\varepsilon/k_BT = -0.023$ ($T = 423.15$ K). The curves from top to bottom correspond to $\varepsilon_{11}/k_BT = 0.45$, 0.47, 0.5, and 0.6. The polymerization indices of two blend components are $N_1 = N_2 = 100$. The same $a-c$ model binary blend is employed in Figs. 3–9, 13 and 14. Figs. 3–21 present χ_{eff} or cloud points for $P = 1$ atm. Figs. 3–12 have $T = 423.15$ K

Fig. 4. High molecular weight limit LCT small angle neutron scattering effective interaction parameter $\chi_{eff}(\Phi_1)$. All parameters are the same as in Fig. 3, except the polymerization indices which are taken as $N_1 = N_2 = 10^4$. The latter values well represent the high molecular weight limit $N_\alpha \to \infty$, $\alpha = 1, 2$

Fig. 5. Molecular weight dependence of the LCT small angle neutron scattering effective interaction parameter $\chi_{eff}(\Phi_1)$ for one of the four model examples from Fig. 3 ($\varepsilon_{11} = 0.47k_BT$). The curves are ——— $N_1 = N_2 = 10^4$, · · · · $N_1 = N_2 = 500$, and – – – – $N_1 = N_2 = 100$

Fig. 6. Same as in Fig. 5 but for $\varepsilon_{11} = 0.6k_BT$

scattering neutrons is always presented first.) All curves have the exchange energy $\varepsilon \equiv \varepsilon_{12} + \varepsilon_{22} - 2\varepsilon_{12} = -0.023k_BT$, $\varepsilon_{22} = 0.6k_BT$ and $T = 423$ K. The curves in Figs. 3 and 4 differ in ε_{11} (and therefore in ε_{12}) to display the resultant changes in the composition dependence of χ_{eff}. The low molecular weights in Fig. 3 introduce a rounding of the $\chi_{eff}(\Phi_1)$ curves at low and high compositions Φ_1,

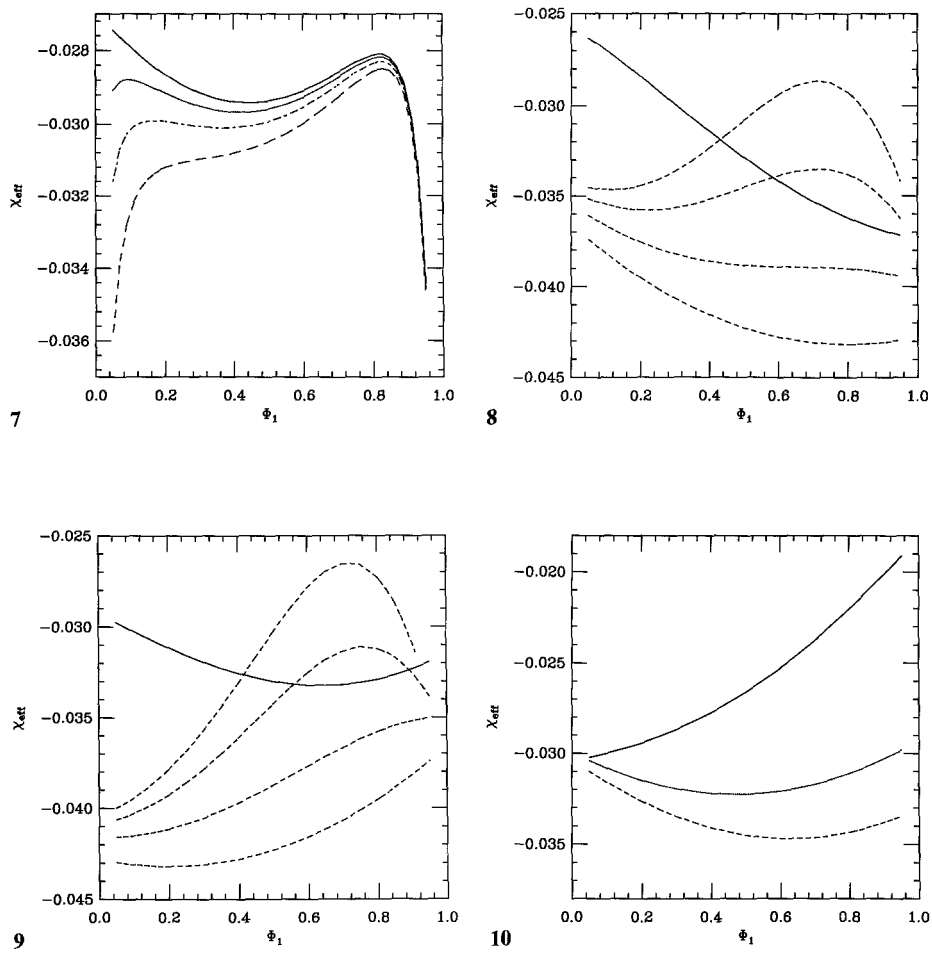

Fig. 7. The LCT small angle neutron scattering effective interaction parameter $\chi_{eff}(\Phi_1)$ for various polymerization indices N_1 of component 1 and constant (but low) polymerization index $N_2 = 100$. The microscopic interaction energies are the same as for one of four examples in Fig. 3 ($\varepsilon_{11}/k_BT = 0.47$, $\varepsilon_{22}/k_BT = 0.6$, and $\varepsilon/k_BT = -0.023$). The curves are labelled as – – – – $N_1 = 50$, – · – · – · – $N_1 = 100$, · · · · $N_1 = 250$, and ——— $N_1 \geqslant 1000$

Fig. 8. High molecular weight limit LCT small angle neutron scattering effective interaction parameter $\chi_{eff}(\Phi_1)$ for various self-interaction energies ε_{11} but constant $\varepsilon_{22}/k_BT = 2.5$ and $\varepsilon/k_BT = -0.023$. The (*dashed*) curves from top to bottom correspond to $\varepsilon_{11}/k_BT = 1.2$, 1.3, 1.5, and 2.5. The figure also shows (*solid line*) an example of an approximately linear dependence of χ_{eff} on Φ_1 that is obtained for $\varepsilon/k_BT = -0.023$, $\varepsilon_{11}/k_BT = 1.5$, and $\varepsilon_{22}/k_BT = 1.0$

Fig. 9. The same as in Fig. 8 but for a model c–a binary blend in which scattering occurs from the c-monomer chains, while it is from the a-monomer chains in Fig. 8

Fig. 10. High molecular weight limit LCT small angle neutron scattering effective interaction parameter $\chi_{eff}(\Phi_1)$ for different model blends but the same three microscopic interaction energies. The curves are labelled as follows: ——— a model a–l binary blend, · · · · a model a–i binary blend with 10 units in the side group, and – – – – a model a–c binary blend. The interaction energies are taken from one of the four examples in Fig. 4 ($\varepsilon/k_BT = -0.023$, $\varepsilon_{11}/k_BT = 0.5$, and $\varepsilon_{22}/k_BT = 0.6$)

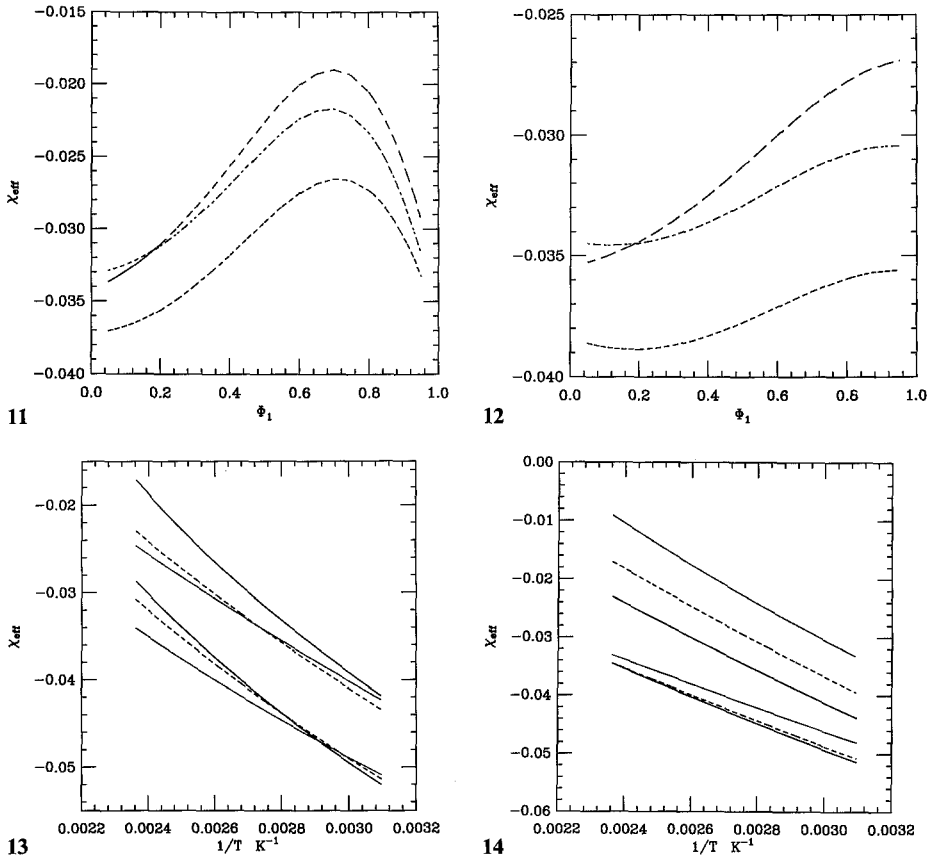

Fig. 11. Variations of high molecular weight limit LCT small angle neutron scattering effective interaction parameter $\chi_{eff}(\Phi_1)$ with monomer structure of the two blend components. The curves are – – – – a model a–c binary blend ($s_1 = 3$ and $s_2 = 5$), – – – – – – a model k–l binary blend ($s_1 = s_2 = 9$), and — — — a model a–l binary blend ($s_1 = 3$ and $s_2 = 9$). The microscopic interaction energies are chosen as $\varepsilon/k_BT = -0.023$, $\varepsilon_{11}/k_BT = 1.2$, and $\varepsilon_{22}/k_BT = 2.5$

Fig. 12. The same as in Fig. 11 but for a different self-interaction energy $\varepsilon_{11}/k_BT = 1.5$

Fig. 13. High molecular weight limit small angle neutron scattering effective interaction parameter χ_{eff} as a function of $1/T$ for various compositions of a model a–c binary blend. The curves are ——— $\Phi_1 = 0.25$, · · · · $\Phi_1 = 0.5$, and – – – $\Phi_1 = 0.75$. The upper set of three curves is generated for $\varepsilon/k_BT_o = -0.023$, $\varepsilon_{11}/k_BT_o = 0.45$, and $\varepsilon_{22}/k_BT_o = 0.6$, while the lower set has $\varepsilon/k_BT_o = -0.023$, $\varepsilon_{11}/k_BT_o = 1.2$, and $\varepsilon/k_BT_o = 2.5$ at $T_o = 423.15$ K

Fig. 14. The same as in Fig. 13 but for different microscopic interaction energy parameters $\varepsilon/k_BT_o = -0.023$, $\varepsilon_{22}/k_BT_o = 0.6$, and $\varepsilon_{11}/k_BT_o = 0.9$ (*upper set*) and $\varepsilon_{11}/k_BT_o = 0.5$ (*lower set*) at $T_o = 423.15$ K

but the central portions of the curves in Fig. 3 have the same shapes as in the high molecular weight limit in Fig. 4. The curves in Fig. 4 are generally parabolic in form, but the center and curvature vary with ε_{11} at constant ε. This behavior is in stark contrast to the usual incompressible blend models in which χ_{eff} is independent of ε_{11} (and molecular weights) at fixed ε. The χ_{eff} in Figs. 3 and 4 differ from ε because of local packing and interaction induced correlations that

are absent in Flory–Huggins theory but that are included in the lattice cluster theory. Figures 3 and 4 also exhibit general variations of $\chi_{eff}(\Phi_1)$ with $|\varepsilon_{11} - \varepsilon_{22}|$ which are in accord with previous trends described [53] in paper II.

Figures 5 and 6 show how varying molecular weight alters the composition dependence of χ_{eff}. These two figures take one example each from the model binary blends of Figs. 3 and 4, respectively, and present $\chi_{eff}(\Phi_1)$ for several molecular weights. The curves from bottom to top in Figs. 5 and 6 correspond to $N_\alpha = 100$, 500, and 10^4 for both $\alpha = 1$ and 2. The rounding of the $\chi_{eff}(\Phi_1)$ curves for low and high Φ_1 disappears at higher M_α, and χ_{eff} tends to increase with M_α (see paper II). Further increasing N_α beyond 10^4 has no influence on χ_{eff}. Molecular weight asymmetry is relevant only when one or more of the components has low molecular weights. This is illustrated in Fig. 7 for a model a–c blends by using $N_1 = 100$ and the set $N_2 = 50$, 100, 250, and 1000, where again the rounding behavior at small and large Φ_1 is a consequence of low molecular weights. Figure 7 also exhibits the general tendency of χ_{eff} to increase with molecular weights [53].

3.4. Dependence of χ_{eff} on monomer structure for high molecular weights

Figure 3 displays some possible shapes generated from our calculations for $\chi_{eff}(\Phi_1)$ when $\varepsilon_{11} \approx \varepsilon_{22}$. However, before studying variations with monomer structure, it is useful to consider the other $\chi_{eff}(\Phi_1)$ curves that are produced when ε_{11} and ε_{22} differ more. Figure 8 employs the same a–c model system as in Fig. 3, but now ε_{22} is much larger and ε_{11} ranges over a wider span. The linear and concave shapes of Fig. 8 depart from those in Fig. 3. Figure 9 has the identical model systems as in Fig. 8, except that the scattering is from the c-monomer chains in Fig. 9, while it is from the a-monomer chains in Fig. 8. The general structures of the curves are similar, but we no longer have $S_{11}(0)$ equal to $S_{22}(0)$ as would be the case for incompressible blends. When the monomer structures range over those in Fig. 2, the $\chi_{eff}(\Phi_1)$ curves are changed quantitatively, but not qualitatively as exhibited in Figs. 10–12. For instance, the bottom curve in Fig. 10 is identical to the second from the bottom curve in Fig. 4 (an a–c model system). The other two curves in Fig. 10 involve model a–l (top) and a–i (middle, for a 10 unit side chain) blends. All three curves in Fig. 10 employ the same energy parameters, polymerization indices, etc.; only the monomer structure changes. The curvature of $\chi_{eff}(\Phi_1)$ is increased by blending a-type chains with the bulkier l or i-type chains. Figure 11 provides another family of $\chi_{eff}(\Phi_1)$ curves that is again produced by only varying monomer structures from a–l, k–l and a–b model blends. Notice that the a–b and k–l blends contain chains with similar monomer structures, while the a–l blend involves very dissimilar monomers. There is not a great difference between the $\chi_{eff}(\Phi_1)$ in Fig. 11 despite the different character of the blends. Many other instances, however, show large departures upon changes in monomer structures. Figure 12 considers the same three model blends as in Fig. 11, where only ε_{11} (and hence ε_{12}) is changed, leading to a substantial alteration in the $\chi_{eff}(\Phi_1)$ curves.

3.5. Temperature dependences of $\chi_{eff}(\Phi_1)$

In general, χ_{eff} at a given composition Φ_1 is close to a linear function of $1/T$ in the high molecular weight limit, with the nonlinearities growing as ε and

$|\varepsilon_{11} - \varepsilon_{22}|$ increase. (Plots of χ_{eff} vs. $1/T$, however, may become very curved when molecular weights are low and when T is near the critical point, but these cases are not discussed further.) What does vary with composition and monomer structure is the slope of χ_{eff} vs. $1/T$. The variation with monomer structure is less significant than that with composition and interaction energies, but this arises partly because of the use of Eq. (3.8) rather than Eq. (3.11) which yields a greater monomer structure dependence. Figures 13 and 14 illustrate the variation of the slope of χ_{eff} vs. $1/T$, as well as the curvature, with composition and microscopic interaction energies. The figures display two examples each, and all of them have structures *a* and *c* of Fig. 2 and the same molecular weights and exchange energy ε; the only differences are the values of ε_{11} and ε_{22} (and hence ε_{12}). The three curves for each set of ε's are for three different compositions ($\Phi_1 = 0.25$, 0.5 and 0.75) and therefore illustrate the variation of the slope with composition. The shifts in overall χ_{eff} between the two sets of curves in each of the figures exhibits the dependence of χ_{eff} on the magnitudes of ε_{11} and ε_{22} at fixed ε, something that is entirely neglected by customary incompressible blend models.

Paper II notes [53] the existence of an interesting quasi-athermal limit in which χ_{eff} is fairly insensitive to temperature, but the ε_{ij} and, in particular, ε are non-zero. However, in the limit of high molecular weights for both blend components, the temperature insensitivity of χ_{eff} arises only when ε is nearly vanishing. On the other hand, the ε_{ij} must definitely be nonzero in order for the blend to be stable at normal pressures [53].

4. Phase diagrams for binary compressible blends: spinodals

It is natural to proceed from a discussion of extrapolated zero angle coherent scattering to a consideration of spinodals as the latter appear when the coherent scattering diverges (the cloud point). The cloud points provide a reasonable approximation to the phase diagrams, and their computation is far simpler than that of the coexistence curves (binodals). All the cloud points computed in this section apply to a pressure of 1 atm. Since the coherent scattering involves a fixed volume in a sample at constant pressure, we employ the cloud point condition of:

$$\frac{1}{S_{11}(0)} = 0. \tag{4.1}$$

but determine the volume V from the equation of state at a pressure $P = 1$ atm. It is extremely important to follow this procedure of evaluating $V(P)$ or equivalently of evaluating $\phi_v(P)$ since use of Eq. (4.1) for arbitrary fixed volumes may lead to spurious additional spinodals that appear for unphysical $P < 0$.

Paper III fits [54] our theory to experimental data on χ_{eff}, ΔH^{mix}, and ΔV^{mix} for PS(D)/PVME blends, so we begin this section by comparing our computations with the experimental cloud points of Han et al. [55] in Fig. 15. The experimental points are the cloud points as determined by extrapolation of data for $S(0)$, while the curve presents our computations using the same molecular weights, monomer structures, and ε_{ij} that are obtained in paper III. The agreement is excellent and must arise in part because of the fit to the neutron scattering data. Discrepancies near the critical point probably arise from the neglected fluctuations. Figure 16 considers the same model blend (with $\varepsilon < 0$) as in Fig. 15 for several molecular weights. The curves show the lower blend critical temperature and the critical composition increasing with decreasing molecular

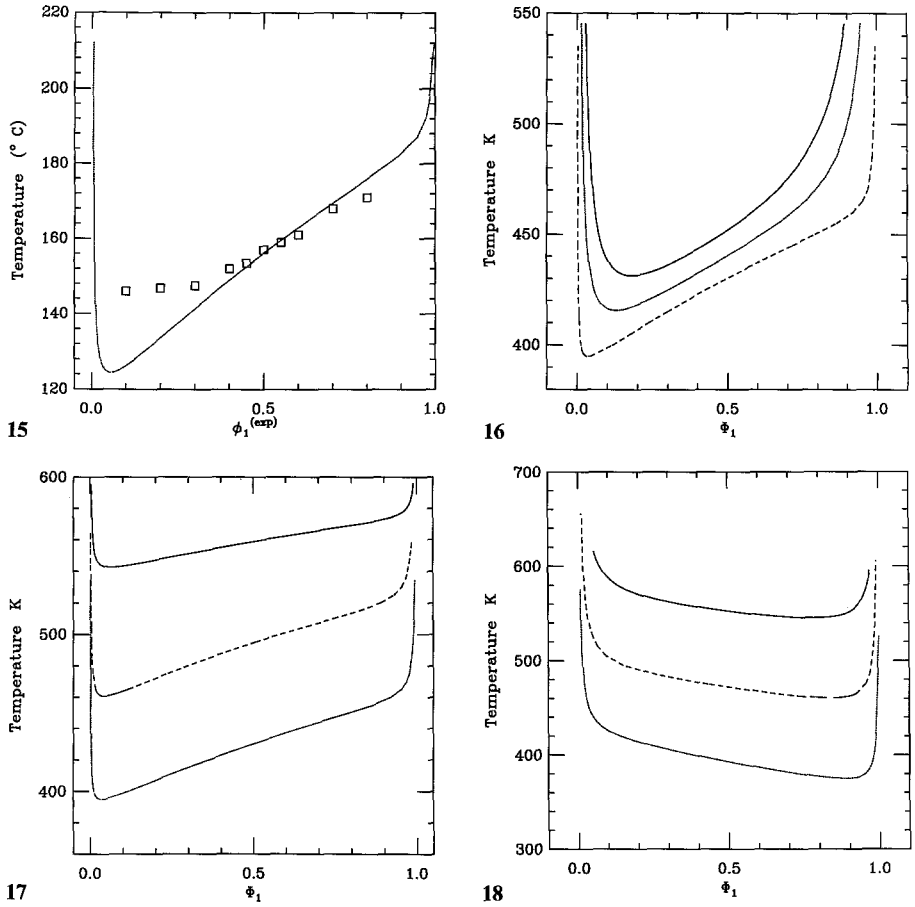

Fig. 15. Comparison of the LCT cloud points for the PSD/PVME blend with experimental data of Han et al. [55] (designated by *squares*). The three microscopic interaction parameters are taken from the fit [54] of the LCT χ_{eff} to experiments for $\chi_{eff}(\Phi_1)$, ΔH^{mix}, and ΔV^{mix} ($\varepsilon/k_BT_o = -0.00721$, $\varepsilon_{11}/k_BT_o = 0.5$, and $\varepsilon_{22}/k_BT_o = 0.56$ at $T_o = 415.15$ K). The model blend is constructed from monomer structures *l* (styrene) and *b* (vinylmethylether)

Fig. 16. The LCT cloud points (spinodal) of a model *l*–*b* blend for different polymerization indices N_α. The curves have $N_1 = N_2 = 10^4$ – – –, $N_1 = N_2 = 10^3$ · · · ·, and $N_2 = N_2 = 5000$ ———. The three microscopic interaction energies are the same as in Fig. 15

Fig. 17. The LCT cloud points (spinodal) for different model blends in the high molecular weight limit. The curves are labelled as ——— a model *l*–*k* blend, – – – a model *l*–*a* blend, and · · · · a model *l*–*b* blend. The interaction energies are identical to those in Fig. 15

Fig. 18. The LCT cloud points (spinodal) in the high molecular weight limit for a model *a*–*l* blend with different self-interaction energies ε_{11} and constant $\varepsilon_{22}/k_BT_o = 0.6$ and $\varepsilon/k_BT_o = -0.001$ ($T_o = 415.15$ K). The curves from top to bottom involve $\varepsilon_{11}/k_BT_o = 1.35$, 1.4, and 1.5 at $T_o = 415.15$ K

weights. The highest molecular weight spinodal in Fig. 16 changes very slightly upon further increasing molecular weights by a factor of 100. Figure 17 displays the variation of the spinodal (for $\varepsilon < 0$) with monomer molecular structures using the same interaction energies as in Fig. 15 but different (high) molecular weights and monomer structures. The curves from top to bottom in Fig. 17 are

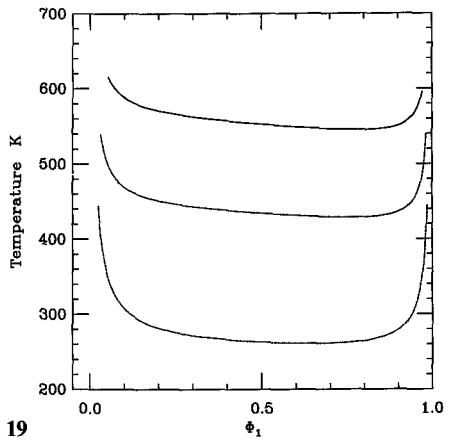

19

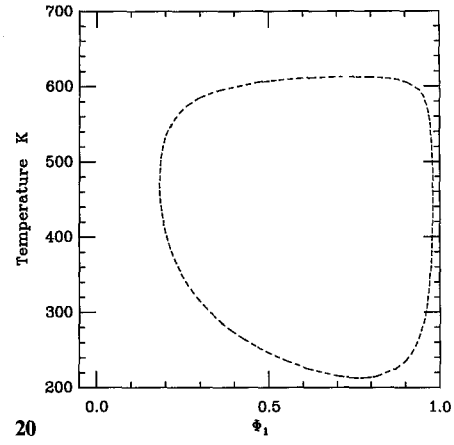

20

Fig. 19. The LCT cloud points (spinodal) for the high molecular weight limit of a model $a-c$ blend for different (negative) exchange energies ε at constant self-interaction energies $\varepsilon_{11}/k_BT_o = 1.35$ and $\varepsilon_{22}/k_BT_o = 1.2$ ($T_o = 415.15$ K). The curves from top to bottom have $\varepsilon/k_BT_o = -0.001$, -0.0005, and -0.0001 at $T_o = 415.15$ K

Fig. 20. The LCT cloud point (spinodal) of a model $a-e$ blend with positive exchange energy $\varepsilon/k_BT_o = 0.12 \times 10^{-4}$, $\varepsilon_{11}/k_BT_o = \varepsilon_{22}/k_BT_o = 0.5$ (at $T_o = 415.15$ K) and polymerization indices $N_1 = 3000$ and $N_2 = 19000$

for $l-k$, $l-a$, and $l-b$ model blends, with identical interaction energies and polymerization indices in all cases. The strong dependence on monomer structures is apparent, but the shapes of the spinodals are similar.

Variations of the spinodal with ε_{11} and ε_{22} at constant $\varepsilon = -0.001k_BT_o$ (with $T_o = 415.15$ K) are presented in Fig. 18 for a model $a-l$ blend. The large temperature scale in Fig. 18 hides the differences in critical compositions $\Phi_1^{(c)}$ and shapes of the three spinodals. From top to bottom the three curves have $\Phi_1^{(c)} = 0.8$, 0.85, and 0.95, respectively. Figure 19 displays the dependence of cloud points on ε for a model $a-b$ blend with other parameters fixed. The expected increase in critical temperature with the net attraction (ε more negative) is evident.

The structure of the spinodals becomes more interesting when the net exchange interaction ε is repulsive ($\varepsilon > 0$). In these cases the molecular weights cannot be too large; otherwise the upper blend critical temperature becomes too high. For instance, the model $a-e$ blend in Fig. 20 exhibits a closed loop phase diagram. When ε is positive and very small, the spinodal has a lower blend critical temperature as in the three curves of Fig. 21a for a model $a-e$ blend in which all parameters but ε remain constant. Making ε more positive drives the critical temperature to lower values, as expected. The spinodals do vary some with monomer structure, but more interesting results are obtained in Fig. 21b as ε is made more repulsive. The cloud point curves in Fig. 21b display both upper and lower critical blend temperatures, and we find similar behavior for a wide variety of model blends. However, the upper critical blend temperature in Fig. 21b probably would lie below the glass transition temperature, while in other examples the lower blend critical temperature would probably lie above the degradation temperature of one or both of the blend components. Nevertheless, the prediction of the possibility for the existence of both critical temperatures in

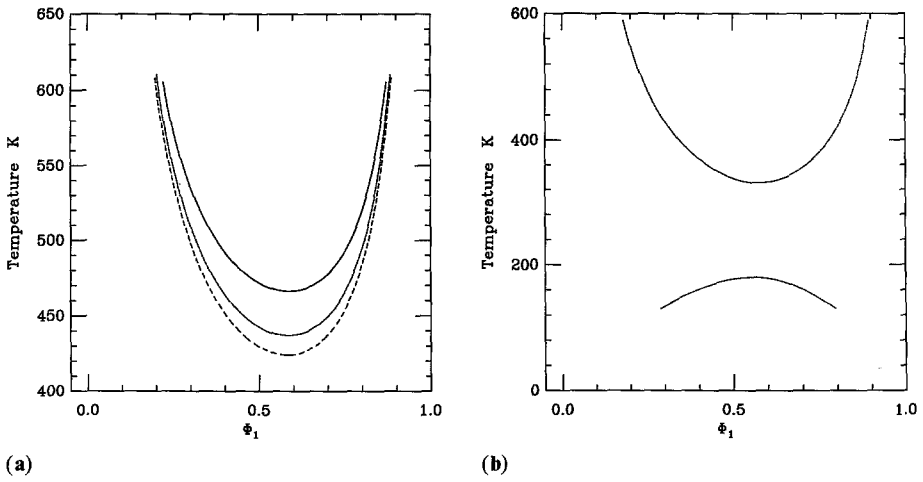

Fig. 21. The LCT cloud points (spinodal) of a model $a-e$ binary blend for various exchange energies ε. The curves have (**a**) ——— $\varepsilon/k_BT_o = -0.5 \times 10^{-4}$, · · · · $\varepsilon/k_BT_o = 0$, and – – – $\varepsilon/k_BT_o = 0.2 \times 10^{-4}$ and (**b**) · · · · $\varepsilon/k_BT_o = 0.12 \times 10^{-3}$ (all energies at $T_o = 415.15$ K). The polymerization indices are chosen as $N_1 = N_2 = 10^3$, while the self-interaction energies are taken as $\varepsilon_{11}/k_BT_o = 1.32$ and $\varepsilon_{22}/k_BT_o = 1.2$ at $T_o = 415.15$ K

blends with no specific interactions is extremely interesting. We have not yet determined the ranges of parameters and monomer structures for which both critical temperatures would lie in conveniently accessible ranges.

5. Discussion

In addition to providing a systematic method for improving the Flory–Huggins approximation to the lattice model of polymer systems, the lattice cluster theory (LCT) enables the inclusion of specific monomer molecular structure and interactions into the theory. An important feature of the LCT is the fact that the free energy of multicomponent polymer systems is obtained as a simple, albeit lengthy, analytical expression that applies for any number of components and for all molecular weights, monomer structures, compositions, temperatures, and nearest neighbor attractive van der Waals interaction energies. This latter feature far outweighs the inherent limitations of any lattice theory as described in previous papers. The present applications of the LCT utilize the simplest possible treatment of the interaction energies in which all portions of a given monomer interact with each other through the same self interaction energy $\varepsilon_{\alpha\alpha}$ and with portions of other species monomers through the same $\varepsilon_{\alpha\beta}$. Thus, a compressible binary polymer blend is characterized by only three independent microscopic interaction energies. It is possible to perform LCT computations using group specific van der Waals energies, but this, of necessity, makes the algebra more lengthy and introduces too many parameters for an initial investigation of the influence of monomer structure on blend properties.

The theory is used here to consider the influence of monomer structure on the composition (Φ_1) dependence of the extrapolated small angle neutron scattering effective interaction parameter χ_{eff} and on cloud points of compressible

binary polymer blends. Paper II begins this study with a consideration of polymers having low molecular weights and rather small and attractive exchange energy $\varepsilon \equiv \varepsilon_{11} + \varepsilon_{22} - 2\varepsilon_{12}$. Low molecular weights are used there to emphasize the molecular weight dependences of χ_{eff}, while the small negative ε are considered as a preliminary to comparisons in paper III with experimental data for PS(D)/PVME blends. The behavior of χ_{eff} with monomer structure, $\varepsilon_{\alpha\beta}$, and temperature is markedly different in the high molecular weight limit than for the low molecular weights studied in paper II. This general behavior is illustrated here using a much wider array of (vinyl) monomer structures than in paper II. Because the calculations here treat higher molecular weights and stable binary blends, it is necessary to perform computations of χ_{eff} for much more attractive ε.

The high molecular weight limit for χ_{eff} still displays a strong dependence on monomer structure, but the dependence is not as dramatic as found in paper II for low molecular weights. However, the definition of the effective χ''_{eff} monomer-monomer interaction parameter implies that χ''_{eff} is affected more by monomer structures because of the explicit factor of $(s_1 s_2)^{1/2}$ in Eq. (3.12). For fixed ε, the shape of the LCT curves for $\chi_{eff}(\Phi_1)$ varies strongly with ε_{11} and ε_{22}, but χ_{eff} is generally found to be a parabolic or linear function of composition Φ_1, in general accord with experimental observations. General trends for the variation of the magnitude of χ_{eff} with molecular weights and interactions $\varepsilon_{\alpha\beta}$ are similar to those delineated in paper II, except that the high molecular weight $\chi_{eff}(\Phi_1)$ do not exhibit the rounding at high and low Φ_1 that is found for low molecular weights. While we do not study the pressure dependence of $\chi_{eff}(\Phi_1)$ for high molecular weights, the behavior is expected to be similar to that described in paper II: Increasing pressure makes the $\chi_{eff}(\Phi_1)$ curve tend more towards the incompressible limit.

Whereas low molecular weights produce a temperature dependence to χ_{eff} that may depart considerably from a linear function of $1/T$, high molecular weights yield a more linear variation, with some curvature due to contributions in the free energy that are bilinear in the $\varepsilon_{\alpha\beta}$, contributions that arise from non-random mixing phenomena. The slopes in plots of χ_{eff} versus $1/T$ generally depend on composition as expected from the nature of the $\chi_{eff}(\Phi_1)$ curves. Paper II defines a quasiathermal blend as one exhibiting a very small T-dependence to χ_{eff} despite having nonzero ε and $\varepsilon_{\alpha\beta}$. This quasiathermal limit occurs for high molecular weights only when ε becomes vanishingly small.

We study the influence of monomer structure and interactions upon the phase diagrams for compressible binary blends. The phase diagrams are represented in terms of the cloud point curves for divergent coherent scattering of radiation. The first computations consider PS/PVME blends in order to compare with the experimental cloud points obtained by Han et al. [55] using monomer structures and microscopic interaction energies $\varepsilon_{\alpha\beta}$ from the fits [54] in paper III to $\chi_{eff}(\Phi_1)$, ΔH^{mix}, and ΔV^{mix}. The agreement is very good considering the deficiencies of the lattice model such as those in taking all junctions to be completely flexible and in neglecting specific interactions for different portions of the vinylmethylether and styrene monomers.

Some general trends in computed cloud point curves are as follows: When the blend has an attractive exchange energy (so $\varepsilon < 0$), there is only a lower critical solution temperature (LCST) which decreases (along with the critical composition) with increasing molecular weights. The cloud point curve is sensitive to the microscopic interaction energies and to the monomer structures. More complicated behavior emerges for positive ε. When $\varepsilon > 0$ is sufficiently small,

there is still only a LCST, but upon increasing ε, both a LCST and an upper solution critical temperature (UCST) may appear. The two critical temperatures, however, do not generally lie between the glass transition and decomposition temperatures. Additional effort is necessary to delineate the conditions under which both critical temperatures may be observable. There is still the expected monomer structure and $\varepsilon_{\alpha\beta}$ dependences, and we have found several instances of closed loop phase diagrams.

The new results in this paper, taken in conjunction with those in papers II and III, indicate a strong sensitivity of blend properties on monomer structures and the importance of treating the blend as compressible. These features provide motivation for further development and extension of the lattice cluster theory.

Acknowledgment. This research is supported, in part, by ONR Grant number N00014-91-J-1442.

References

1. Flory PJ (1953) Principles of polymer chemistry. Cornell University, Ithaca, NY
2. Yamakawa H (1971) Modern theory of polymer solutions. Harper & Row, NY
3. Meyer KH (1939) Z Phys Chem Abt B 44:383
4. Fowler RH, Rushbrooke GS (1937) Trans Faraday Soc 33:1271
5. Chang TS (1939) Proc Cambridge Philos Soc 35:265
6. Miller AR (1942) Proc Cambridge Philos Soc 38:109
7. Flory PJ (1941) J Chem Phys 9:660
8. Flory PJ (1956) Proc R Soc, London A 234:60
9. Flory PJ Proc Natl Acad Sci, USA 79:451
10. Huggins ML (1941) J Chem Phys 9:440; (1942) J Phys Chem 46:151; (1943) Ann NY Acad Sci 44:431
11. Kirkpatrick S (1973) Rev Mod Phys 45:574
12. Gibbs JH, DiMarzio EA (1958) J Chem Phys 28:373; (1958) Ibid 28:807; (1963) J Polym Sci Part A 1:1417
13. DiMarzio EA (1961) J Chem Phys 35:658
14. Cotter MA, Martire DE (1969) Mol Cryst Liq Cryst 7:295; Cotter MA (1976) Mol Cryst Liq Cryst 35:33
15. Alben R (1971) Mol Cryst Liq Cryst 13:193
16. McCraken FL (1978) J Chem Phys 69:5419
17. Baumgartner A (1985) J Phys (Paris) Lett 46:L659
18. Ciferri A, Flory PJ (1959) J Appl Phys 30:1498
19. Allen G, Tanaka T (1977) Macromolecules 10:426
20. Scott RL (1949) J Chem Phys 17:279
21. de Gennes PG (1977) J Phys (Paris) Lett 38:L441; (1978) J Polym Sci (Phys) 16:1883
22. Brandup J, Immergut EH (eds) (1975) Polymer handbook. Wiley, NY IV:131 and references therein
23. Eichinger BE, Flory PJ (1968) Trans Faraday Soc 64:2035, 2053, 2061, 2066
24. Flory PJ (1970) Discuss Faraday Soc 49:7
25. Scholte ThG (1970) J Polym Sci A-2 8:841
26. Murray CT, Gilmer JW, Stein RS (1985) Macromolecules 18:996
27. Koningsveld R, Kleitjens LA (1971) Macromolecules 4:637
28. Kurata M, Tamura M, Watari T (1955) J Chem Phys 23:991
29. Guggenheim EA (1944) Proc R Soc London A 183:203
30. Patterson D, Delmas G (1970) Ibid 49:98
31. Sanchez IC, Lacombe RH (1978) Macromolecules 11:1145
32. Prigogine I, Trapeniers N, Mathot V (1953) Discuss Faraday Soc 15:93
33. Panayioutou CG (1987) Macromolecules 20:861

34. Baumgartner, Binder K (eds) (1984) Applications of the Monte Carlo method in statistical physics. Springer, NY and references therein
35. Dickman R, Hall CK (1986) J Chem Phys 85:3023
36. Sariban A, Binder K (1987) J Chem Phys 86:5859
37. Freed KF (1987) Renormalization group theories of macromolecules. Wiley-Interscience, NY
38. Freed KF (1985) J Phys A 18:871
39. Bawendi MG, Freed KF, Mohanty U (1986) J Chem Phys 84:7036
40. Bawendi MG, Freed KF (1988) J Chem Phys 88:2741
41. Bawendi MG, Freed KF, Mohanty U (1987) J Chem Phys 87:5534
42. Nemirovsky AM, Bawendi MG, Freed KF (1987) J Chem Phys 87:7272
43. Freed KF, Pesci AI (1987) J Chem Phys 87:7342
44. Pesci AI, Freed KF (1989) J Chem Phys 90:2003
45. Bawendi MG, Freed KF (1986) J Chem Phys 85:3007
46. Bawendi MG, Freed KF (1987) J Chem Phys 86:3720
47. Ramond P (1981) Field theory, a modern primer. Benjamin/Cummings, Reading, MA
48. Itzykson C, Zuber J (1980) Quantum field theory. McGraw-Hill, NY
49. Freed KF (1972) Adv Chem Phys 22:1
50. Freed KF, Bawendi MG (1989) J Phys Chem 93:2193
51. Dudowicz J, Freed KF, Madden WG (1990) Macromolecules 22:4803
52. Dudowicz J, Freed KF (1991) Macromolecules 24:5076
53. Dudowicz J, Freed MS, Freed KF (1991) Macromolecules 24:5096
54. Dudowicz J, Freed KF (1991) Macromolecules 24:5112
55. Han CC, Baurer BJ, Clark JC, Muroga Y, Okada M, Tran-Cong Q, Sanchez IC (1988) 29:2002